

## Nucleation Effects on Tip-Gap Cavitation.

P. S. Russell<sup>1</sup>, L. Barbaca<sup>1</sup>, J. A. Venning<sup>1</sup>, B. W. Pearce<sup>1</sup>, and P. A. Brandner<sup>1</sup>

<sup>1</sup> National Centre for Maritime Engineering & Hydrodynamics  
Australian Maritime College  
University of Tasmania, Launceston TAS 7250, Australia

### Abstract

Cavitation in tip leakage flows have been investigated in a water tunnel for different concentrations of free-stream cavitation nuclei. High-resolution still photography exhibits similar cavitation topology overall. However, hydro-acoustic measurements reveal stark differences in the desinent extinction of cavitation when different levels of active nuclei are present. Results quantify the anticipated challenges in designing enclosed propulsors and turbo-machinery that operate in flows with varying susceptibility to cavitation.

### Keywords

Cavitation; Nuclei; Tip-Gap Flow

### Introduction

Flow between the tip of a rotating blade and a static casing, referred to as Tip Leakage Flow (TLF), has received considerable attention in research due to its impact on efficiency and quiet operation of ducted propulsors and turbo-machinery. Results from experimentation have explored most flow parameters affecting the cavitation performance including Reynolds number scale effects [1], inlet boundary layer thickness [2], and gap/clearance height [3]. However, the influence of cavitation nuclei concentration on the extent of cavitation in these flows, particularly the precise locations of cavitation inception and desinence, are not yet well understood.

Conventional wisdom would indicate that the region of lowest pressure is found in the core of the Tip Leakage Vortex (TLV), and hence is the principle location for cavitation near inception or desinence. However, some research suggests that near the free-stream pressure threshold, cavitation may occur first in smaller secondary vortices as they become stretched during the merging of the primary tip leakage vortex and the much weaker trailing edge vortex [4, 5]. Similar vortex bridging is observed in these experiments, formed between the TLV and a Tip Separation Vortex (TSV) occurring in the clearance between the tip and the wall. Example TSV and TLV cavitation are presented in Figure 1. Flow separation and the development of a TSV is found on sharp-edged blade tips [6], which are still often used in pumps and turbo-machinery.

For such a flow the effect of free-stream nuclei concentration, on desinent behaviour is investigated by slowly raising the pressure around a cavitating hydrofoil for two free-stream populations: A low concentration typical of the nuclei found in the ocean many tens of meters below the surface, and a high concentration with a population similar to near-surface conditions.

### Experiment

The experiments were performed in the University of Tasmania variable pressure water tunnel. The tunnel test-section is  $0.6 \times 0.6$  m square at the entrance, by 2.6 m long. The test-section ceiling is horizontal with the floor sloping 20 mm over the length to maintain nominally constant speed and a zero-stream-wise pressure gradient. The operating velocity and pressure are controlled independently, with ranges from 2 to 12 m/s and 4 to 400 kPa absolute respectively. The tunnel volume is  $365 \text{ m}^3$  and is filled with demineralised water. Optical access is provided through acrylic windows on each side of the test-section, and a long acrylic window in the test section ceiling.

The test-section absolute pressure is measured, depending on the value, from low- or high-range Siemens Sitrans-p absolute pressure transducers models 7MF4333-1FA02-2AB1 (range 0-130 kPa) and 7MF4333-1GA02-2AB1 (range 0-400 kPa), with estimated precision of 0.13 and 0.48 kPa respectively. The test-section velocity is measured from calibrated contraction differential pressure. Depending on the value, either low- or high-range Siemens Sitrans-p differential pressure transducers models 7MF4333-1DA02-2AB1-Z (range 0-25 kPa) and 7MF4333-1FA02-2AB1-Z (range 0-160 kPa) are used, with estimated precision of 0.007 and 0.018 m/s respectively. The test section velocity has been measured to be spatially uniform to within 0.5%, has a temporal variation of less than 0.2%, and a free stream turbulence intensity of 0.5%. The dissolved gas content of the water is measured using an Endress+Hauser OxyMax WCOS 41 membrane sensor. Further details on the facility can be found in [7].

The experimental setup has been developed to study cavitation in the gap flow between a stationary hydrofoil and the ceiling of the tunnel test-section, as schematically represented in

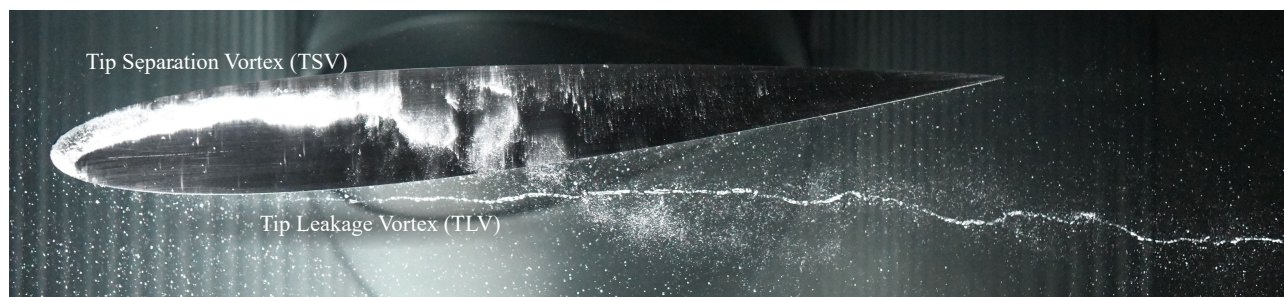


Figure 1. Heavily nucleated tip-gap flow with cavitation in the Tip Separation Vortex (TSV) and Tip-Leakage Vortex (TLV) for chord based Reynolds number of  $Re = 2.5 \times 10^6$  and cavitation number  $\sigma = 1.3$ , with a tip gap height to hydrofoil thickness ratio of  $\tau = 0.28$ .

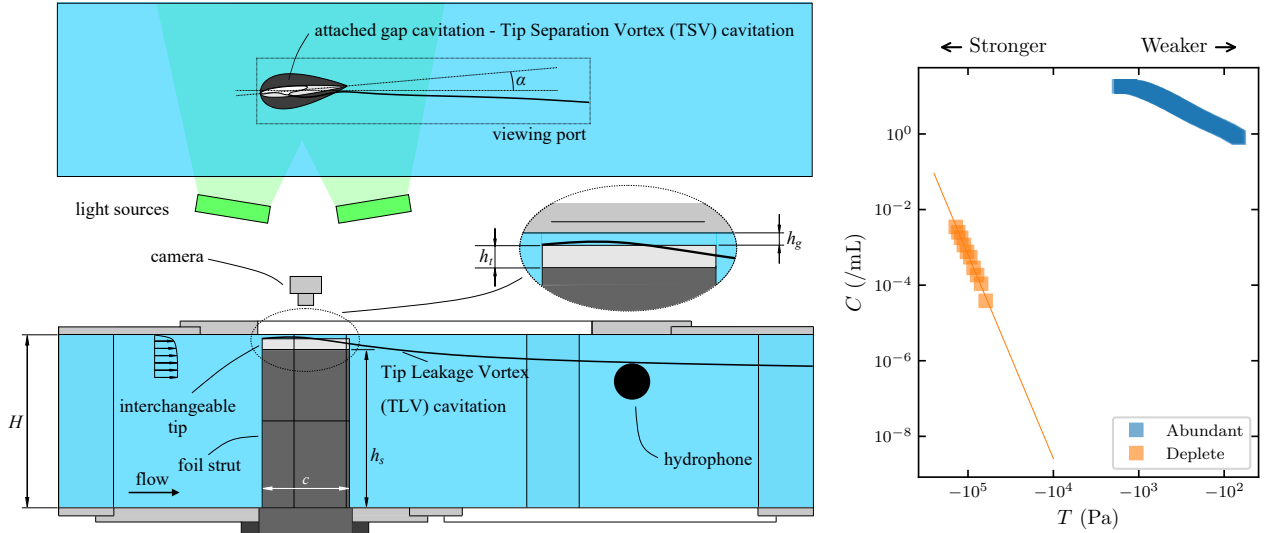


Figure 2. Schematic of the experiment along with the typical nuclei concentrations measured in the tunnel for the background (nuclei deplete) and highly seeded (abundant) populations.

Figure 2. The hydrofoil and mounting disk are machined from a  $\phi 320 \times 650$  mm long stainless steel billet. The hydrofoil blade has a span,  $h_s$ , of 554 mm and a chord,  $c$ , of 300 mm. The blade consists of a 234 mm parallel NACA 0012 section at the tip, and from the mid span tapers to a NACA 0040 section at the base in order to increase the model stiffness and avoid vibration. The model is mounted rigidly to the bottom of the test-section. To investigate the effect of tip clearance on the flow the model can be equipped with interchangeable tip section of span  $h_t$ , enabling the experiments with the tip clearance,  $h_g$ , ranging from 2 to 50 mm. For this experiment a tip with a clearance of 10 mm was used, and when non-dimensionalised by the maximum hydrofoil thickness ( $t$ ), produced a gap ratio of  $\tau = h_g/t = 0.278$ . Both the hydrofoil blade and the interchangeable tips have squared edges. The hydrofoil leading edge is located  $\approx 900$  mm downstream of the test-section entrance with the unperturbed incoming wall boundary layer thickness at that position being  $\delta = 19$  mm. Experiments were performed with hydrofoil incidence,  $\alpha = 5$  deg.

High-resolution still images of cavitation in the gap and the hydrofoil near wake region were captured using a Nikon D850 DSLR camera equipped with a Nikon Nikkor AF 35 mm 1:2D lens. The camera was mounted above the tunnel test-section, with the optical access to the gap provided through a 1150 mm long by 215 mm wide acrylic window in the test-section ceiling. The exposure was controlled using simultaneously triggered stroboscopic flashes — Drello 3018/HL4037 and Drello 1018/LE4040 — mounted to the side of the tunnel test-section, level with the tip gap. To reduce the glare and reflections, the flash-lamps were masked using a curtain to allow only a narrow band of light to pass along the ceiling.

Acoustic measurements were obtained using a Brüel & Kjær Type 8103 hydrophone (voltage sensitivity  $25.1 \mu\text{V}/\text{Pa}$ ) mounted in a flooded cavity (kept at the same pressure as the tunnel test conditions) beneath a 10 mm polyurethane diaphragm, with a 149 mm sensing diameter. The hydrophone was mounted in the side wall, 150 mm below the ceiling and approximately 3.5 chord lengths downstream of the hydrofoil trailing edge. The signal was conditioned with a Brüel & Kjær Nexus conditioner and amplifier, which was also used to apply a 0.1 Hz - 100 kHz bandpass filter. The filtered signal was

acquired using a National Instruments PXIe-4497 card at a sampling rate of 204.8 kHz.

The experiments were performed for a fixed chord based Reynolds numbers,  $Re = Uc/\nu = 2.5 \times 10^6$ , where  $U$  is the free-stream flow velocity and  $\nu$  is the kinematic viscosity of the water. The cavitation number is defined as  $\sigma = (p - p_v)/0.5\rho U^2$ , where  $p$  is the static pressure at the test-section ceiling,  $p_v$  is the vapour pressure and  $\rho$  is the water density. The two nuclei concentrations used in these experiments were measured separately to these tests. The natural (deplete) population, has been measured extensively [8], via mechanical activation with a Cavitation Susceptibility Meter (CSM) and has a sparse concentration of order  $C \approx 10^{-3} \text{ mL}^{-1}$ . The second (abundant) population has been measured using interferometric Mie-Scattering Imaging and has a typical concentration of  $C = 1.5 \times 10^1 \text{ mL}^{-1}$ . The distribution of bubble size and concentrations for each total concentration are presented cumulatively with respect to their equivalent critical tension in Figure 2. The sparse population of smaller bubbles leads to “stronger” water, while seeded water can sustain less tension.

Seeding of the tunnel flow with nuclei is realized using an array of micro-bubble generators positioned in the plenum upstream of the tunnel honeycomb and contraction. The generators operating principle is based on rapid expansion of supersaturated water in a confined turbulent jet. Supersaturated water is expanded through a 0.5 mm by 0.3 mm long orifice into a 1.2 mm by 200 mm long hypodermic tube, where micro-bubbles form in shear layer cavities. Bubble production is characterised by the driving pressure,  $\Delta p_{gen} = p_{sat} - p_{plenum}$ , and generator cavitation number  $\sigma_{gen} = (p_{sat} - p_{plenum})/\Delta p$ . At peak operation, generators produce a poly-disperse plume of micro-bubbles 2-200  $\mu\text{m}$  in diameter [9]. While generator parameters are coupled to the tunnel pressure and velocity — through the pressure in the plenum — a study of the bubble populations produced in the test section show that only minor changes are found when a constant generator-cavitation number of  $\sigma = 0.25$  is maintained [10]. To achieve this the saturation vessel pressure was raised in conjunction with the tunnel pressure, with adequate time between data sampling to allow for en-gassing of the saturation vessel to take place.

## Results

For both nuclei concentrations, the cavitation number was controlled by slowly raising the tunnel pressure from a condition where extensive cavitation was visible, until shortly after desinence. The visible and acoustic characteristics of this change were compared.

The enlarged image in Figure 1 exhibits the main topological features of the flow. The Tip Separation Vortex (TSV) forms in the clearance flow from the sharp-edged end of the hydrofoil. This vortex and bubbles condensed from cavitation are swept across the end of the hydrofoil by the leakage flow and are wound around the Tip Leakage Vortex (TLV). Bubble cloud structures immediately after condensation of the TSV indicate this cavity fluctuates, undergoing shedding of some kind. Only marginally present in Figure 1, but observed in other images is an induced secondary vortex that may also cavitate, seen just above the bubble clouds from the TSV. The unsteadiness in this flow causes the TLV to meander. Some bubbles are entrained into the TLV from the TSV and at very low cavitation numbers the TSV was observed to begin merging with the TLV near the trailing edge of the hydrofoil at this Reynolds number. At this cavitation number, primary seeding of the TLV is from a thin line of bubbles drawn from the gap cavity at the leading edge. At higher  $\sigma$  this diminishes until bubbles from the free-stream and TSV collapse dominate seeding of the TLV.

Acoustic spectra demonstrating the background noise and acoustic emission during cavitation for both the abundant and deplete populations are plotted in Figure 3. Acoustic data was directly measured without development and application of an acoustic transfer function. With only the natural tunnel nuclei population, no cavitation occurred, and the background flow and tunnel noise was recorded. When the nuclei concentration was increased — but no cavitation present — a lift in the spectra for  $f > 5$  kHz was present due to noise produced by the nuclei seeding generators. At low pressure, for  $\sigma = 2.5$ , cavitation was visually observed, and both spectra are similar regardless of nuclei population. A sharp peak at 650 Hz with associated first and second harmonics are visible, as well as a large broadband increase in power for frequencies above approximately 200 Hz. However, a slight difference is present at higher frequencies with marginally increased power in the deplete spectra for frequencies above approximately 10 kHz. This occurs due to the

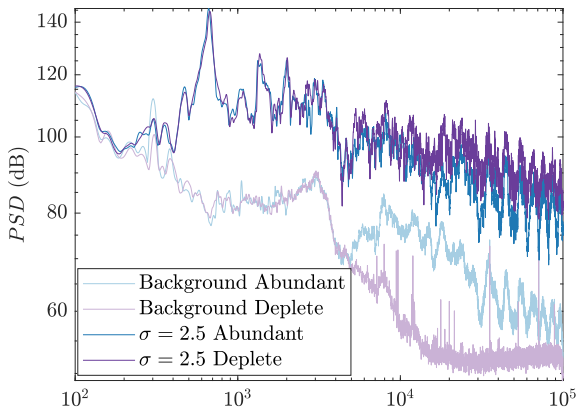


Figure 3. Acoustic spectra demonstrating the background noise and acoustic emission during cavitation for both the abundant and deplete populations, sampled at  $f_s = 204.8$  kHz. For the low nuclei (deplete) population, the background noise conditions without cavitation was  $\sigma = 3.2$ . For the high nuclei (abundant) population, conditions for the background noise without cavitation was  $\sigma = 6.0$ .

damping provided by increased gas within bubbles supplied by the initial bubble volumes for the highly nucleated flow. Acknowledging this minor difference, cavitation at this  $\sigma$  is very similar. This is supported visually by the still images, presented in Figure 4 (a-d).

To examine differences across cavitation number, still images for  $\sigma = \{1.1, 1.5, 2, 2.5\}$  along with spectrograms with increasing  $\sigma$  for both abundant and deplete flow are presented in Figure 4). These spectrograms mirror the test procedure where  $\sigma$  was slowly raised. Similar trends were observed for both the deplete and abundant flow for  $\sigma < 3$ . A strong peak that increases with cavitation number is present at 200 Hz for  $\sigma = 1.5$  up to 900 Hz for  $\sigma = 2.8$ . While cavitation and bubble capture were observed in the tip leakage vortex, still images indicate the change in frequency of this acoustic peak with  $\sigma$  is associated with the change in volume of the TSV cavity. In addition, while the frequency changes with  $\sigma$  the strength of this peak appears tied to the aspect ratio of the TVC cross section. For low  $\sigma$  where the cavity covers a portion of the hydrofoil tip larger than the gap height of 10 mm the peak begins to spread its power over a broader band of frequencies. Further testing incorporating high-speed video is planned to examine noise generation mechanisms are associated with cavity shedding or resonant mode shapes of the cavity, as has been previously investigated for isolated vortex cavitation [11].

For the deplete case a sharp drop in power at  $\sigma = 3.2$  due to abrupt desinence of the TSV cavity was measured (Figure 4e). Just prior to this the strong peak begins to spread in frequency, distributing its power. In contrast, for the flow abundant with nuclei desinence is more gradual. The role of nuclei in this behavior is readily reasoned. In the deplete case cavitation is sustained or re-nucleated by small cavities or bubbles trapped in the separated flow, but pressure within the flow fluctuates. Once momentary desinence occurs, without free-stream nuclei to reseed it, no new cavities form. Conversely, free-stream nuclei in the abundant flow continue to be activated by the fluctuating pressure in the TSV with fewer, and smaller, activation events. Small activations of this kind can be observed in the TSV in (Figure 4d) whereas cavitation is absent in the accompanying deplete case (Figure 4c).

## Conclusions

Visual and acoustic differences in tip-gap cavitation desinence for two free-stream nuclei populations have been investigated experimentally. The topology and noise emitted from cavitation remain similar when separated flow in the gap develops for both the abundant and deplete nuclei populations. Wrapping of the tip separation vortex around the tip leakage vortex, and merging of the two can be visualised with cavitation. A strong peak in acoustic emission was observed for both nuclei populations for  $1.5 < \sigma < 2.8$ . This is associated with cavitation in the gap separation vortex, and the frequency reduces as the cavity size increases. However, there are stark difference in desinent behaviour. For deplete flows cavitation desinence is sudden, while for abundant flow it is gradual.

## Acknowledgements

This project was supported by the US Office of Naval Research (Dr. Ki-Han Kim) and ONR Global (Dr. Sung-Eun Kim) through NICOP S&T Grant no. N62909-19-1-2062, and the 2019 U.S. Multidisciplinary University Research Initiative (MURI), through the Australian Defence Science and Technology Group (Dr. Dev Ranmuthugala and Dr. David Clarke). The authors are grateful for technical assistance provided by Mr. Steven Kent and Mr. Robert Wrigley during experiments.

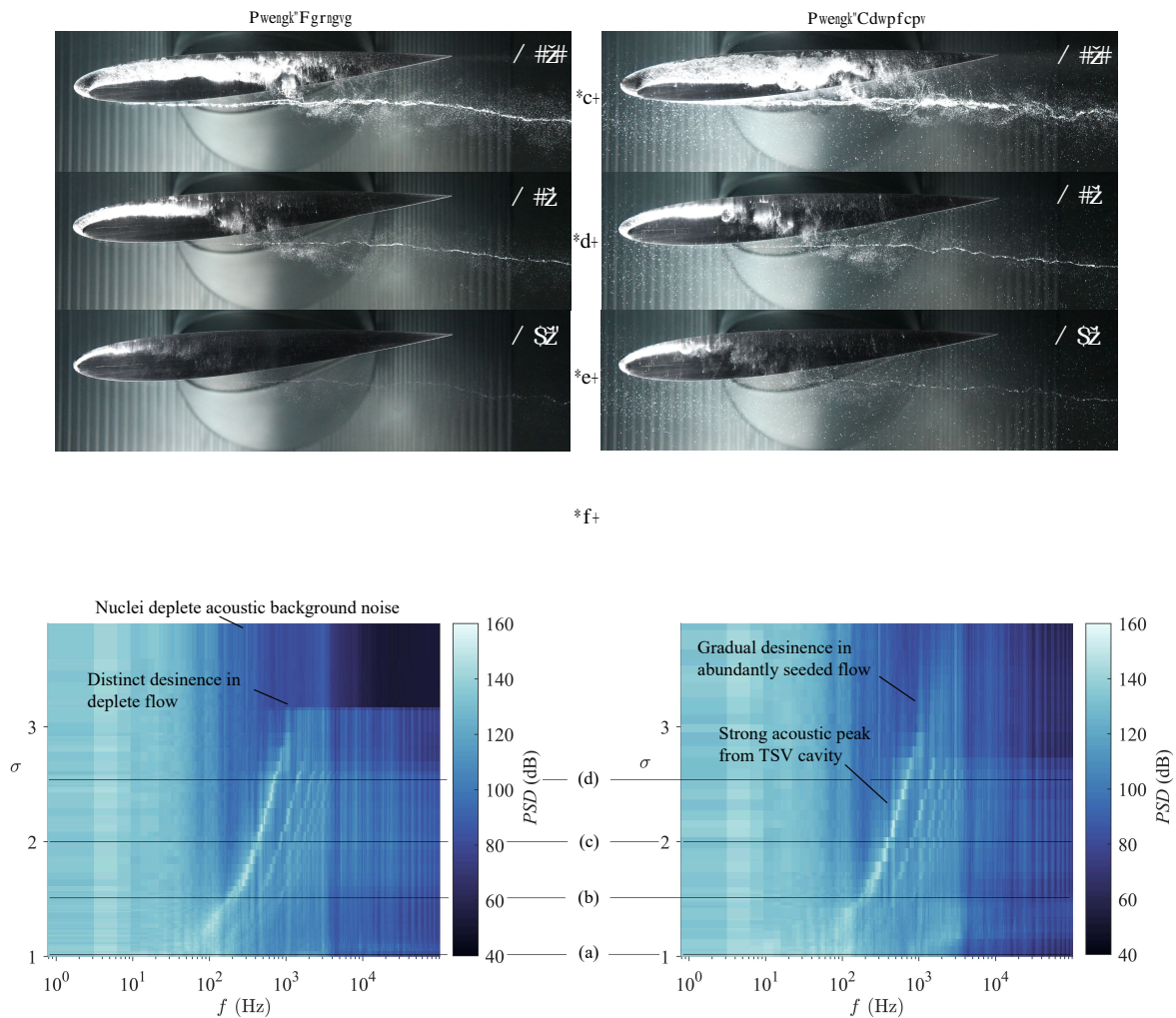


Figure 4. Still images from deplete (left) and abundant populations (right) for four cavitation numbers (a-d). Spectrograms of acoustic data for  $1 < \sigma < 3.9$  for both nuclei deplete and abundant flows are presented below (e-f).

## References

- [1] Oweis, G.F., Fry, D., Chesnakas, C.J., Jessup, S.D., and Ceccio, S.L. (2006). Development of a Tip-Leakage Flow—Part 1: The Flow Over a Range of Reynolds Numbers *Journal of Fluids Engineering*, 128(4), 751–764.
- [2] Chan, J.K.K., Yaras, M.I., and Sjolander, S.A. (1994). Interaction between inlet boundary layer, tip-leakage and secondary flows in a low-speed turbine cascade. in *Turbo Expo: Power for Land, Sea, and Air*. ASME Paper 94-GT-250
- [3] Dreyer, M., Decaix, J., Münch-Alligné, C., and Farhat, M. (2014) Mind the gap: a new insight into the tip leakage vortex using stereo-PIV *Experiments in Fluids*, 55(11), 1849
- [4] Oweis, G. F., and Ceccio, S. L. (2005). Instantaneous and time-averaged flow fields of multiple vortices in the tip region of a ducted propulsor. *Experiments in fluids*, 38(5), 615-636.
- [5] Chesnakas, C. J., and Jessup, S. D. (2003). Tip-vortex induced cavitation on a ducted propulsor. in *Fluids Engineering Division Summer Meeting* 36967, 257–267).
- [6] Decaix, J., Balarac, M., Dreyer, M., Farhat, M., and Münch, C. (2015) RANS and LES computations of the tip-leakage vortex for different gap widths. *Journal of Turbulence*, 16(4), 309–341, (DOI:10.1080/14685248.2014.984068)
- [7] Brandner, P.A., Lecoffre, Y., and Walker, G.J. (2007) Design considerations in the development of a modern cavitation tunnel. in *Proceedings of the 16th Australasian Fluid Mechanics Conference (16AFMC)*, 630–637.
- [8] Venning, J.A., Khoo, M.T., Pearce, B.W., Brandner, P.A. (2018) Background nuclei measurements and implications for cavitation inception in hydrodynamic test facilities. *Experiments in Fluids*, 59(4), 71.
- [9] Giosio, D., Pearce, B., and Brandner, P. (2016) Influence of pressure on microbubble production rate in a confined turbulent jet. in *20th Australasian Fluid Mechanics Conference (20AFMC)*, 1–4
- [10] Russell, P.S., Barbaca, L., Venning, J.A., Pearce, B.W., and Brandner, P.A. (2020) Measurement of Nuclei Seeding in Hydrodynamic Test Facilities. *Experiments in Fluids* 61(3), 1–18.
- [11] Pennings, P.C., Bosschers, J., Westerweel, J., and van Terwisga, T.J.C. (2015) Dynamics of isolated vortex cavitation. *Journal of Fluid Mechanics* 778, 288–313.